

Dust Grain Evolution in Spatially Resolved T Tauri Binaries¹

Andrew J. I. Skemer¹, Laird M. Close¹, Thomas P. Greene², Philip M. Hinz¹, William F. Hoffmann¹ and Jared R. Males¹

¹*Steward Observatory, Department of Astronomy, University of Arizona, 933 N. Cherry Ave, Tucson, AZ 85721*

²*NASA Ames Research Center, Moffett Field, CA 94035*

ABSTRACT

Core-accretion planet formation begins in protoplanetary disks with the growth of small, ISM dust grains into larger particles. The progress of grain growth, which can be quantified using $10\mu\text{m}$ silicate spectroscopy, has broad implications for the final products of planet formation. Previous studies have attempted to correlate stellar and disk properties with the $10\mu\text{m}$ silicate feature in an effort to determine which stars are efficient at grain growth. Thus far there does not appear to be a dominant correlated parameter. In this paper, we use spatially resolved adaptive optics spectroscopy of 9 T Tauri binaries as tight as $0.25''$ to determine if basic properties shared between binary stars, such as age, composition, and formation history, have an effect on dust grain evolution. We find with 90-95% confidence that the silicate feature equivalent widths of binaries are more similar than those of randomly paired single stars, implying that shared properties do play an important role in dust grain evolution. At lower statistical significance, we find with 82% confidence that the secondary has a more prominent silicate emission feature (i.e., smaller grains) than the primary. If confirmed by larger surveys, this would imply that spectral type and/or binarity are important factors in dust grain evolution.

1. Introduction

The core-accretion model for planet formation (e.g., Lissauer & Stevenson 2007) is a multi-step process beginning with the agglomeration of small interstellar medium (ISM)

¹The observations reported here were obtained at the MMT Observatory, a facility operated jointly by the Smithsonian Institution and the University of Arizona.

dust grains into larger particles. Eventually, these particles reach the size of planetesimals and gravitationally attract each other and their surrounding gas. Planet formation must occur quickly, as several physical processes are able to disperse the gas and dust of the protoplanetary disk. Consequently, the timescale over which each aspect of core-accretion occurs is critical to the final outcome of the planet formation process. The first step of core-accretion, where small ISM dust grains agglomerate into larger particles, is of particular importance as it sets the conditions for all of the other core-accretion steps.

Dust grain properties can be studied at a variety of wavelengths and locations in the disk (Natta et al. 2007). Visible and near-infrared scattered light imaging can be used to study the grain sizes of submicron and micron surface dust at large radial distances. Mid-infrared spectroscopy of the $10\mu\text{m}$ and $20\mu\text{m}$ silicate emission features can be used to determine the size and composition of submicron and micron sized surface dust at small radial distances. Far-infrared and millimeter continuum observations probe deep into the disk mid-plane over the full radius of the disk and can be used to determine the size distribution and total mass of mm-cm dust grains. Although these observations probe different grain sizes at different locations in the disk, it appears that they are somewhat correlated. In particular, the equivalent width of the $10\mu\text{m}$ silicate feature is correlated with the slope of the submillimeter spectral energy distribution (SED), implying that dust grain growth proceeds concurrently through its various phases (Lommen et al. 2010). Additionally, the shape of the $10\mu\text{m}$ silicate feature is correlated with its amplitude, likely due to the simultaneous development of large amorphous grains and crystalline grains (van Boekel et al. 2003; Przygodda et al. 2003; Apai et al. 2005).

Our current understanding of dust grain growth is that it begins during the Class II phase of star/planet formation, once the dust is collected into a circumstellar disk (Beckwith & Sargent 1991; Ossenkopf & Henning 1994; Kruegel & Siebenmorgen 1994). At this point, dust grains are expected to coagulate and settle rapidly ($\sim 10^3 - 10^6$ years depending on model assumptions; Dullemond & Dominik 2005; Brauer et al. 2008). However, Class II objects over a wide span of ages ($\sim 0.5-10$ Gyr) have a diverse set of dust grain properties, implying that dust evolution is not simply a function of age (Meeus et al. 2001; Przygodda et al. 2003; van Boekel et al. 2005; Apai et al. 2005; Kessler-Silacci et al. 2006; Furlan et al. 2009; Oliveira et al. 2011). Even within individual clusters, which are approximately coeval, there is no apparent correlation between mid-infrared dust properties and stellar mass, luminosity, stellar accretion or disk mass (Sicilia-Aguilar et al. 2007; Watson et al. 2009). Over a large range of masses, taken between stars in different clusters with different ages, there appears to be a weak correlation between mass and silicate feature strength (Kessler-Silacci et al. 2006; Pascucci et al. 2009), which might be the result of another spectral-type dependent factor, such as X-rays or the location of the silicate emission zone (Glauser et al. 2009;

Kessler-Silacci et al. 2007). However, the general diversity of dust properties between similar stars of similar ages suggests that additional properties are needed to explain the evolution of the dust.

One way to isolate which stellar properties are important for dust grain evolution is to observe the dust grain properties of coeval young binaries. Binaries share certain properties, such as age, composition and formation history, which are difficult to ascertain in individual stars. If these properties are important for dust grain evolution, then we expect the dust to be similar in binary pairs. However, if these properties are unimportant, then the binary stars will have a random distribution of dust characteristics, similar to those observed in single stars. Additionally, if the shared properties are important, they might be hiding correlations between other stellar parameters and dust grain characteristics, which can be uncovered by taking advantage of the coevality of binaries.

In this paper (and including the results of Skemer et al. 2010), we present spatially resolved $10\mu\text{m}$ silicate spectroscopy of 8 Taurus-Aurigae² binaries, which triples the sample size of spatially/spectrally resolved binaries in a single cluster at mid-infrared wavelengths. Small diameter space-based telescopes are unable to perform high spatial resolution ($\lesssim 2-3''$) observations in the mid-infrared ($>8\mu\text{m}$) due to their large diffraction limits (additionally, the Infrared Spectrograph, IRS, on *Spitzer* is no longer operational, so mid-infrared spectroscopy is not currently accessible from space). Ground-based observatories have much larger diameters but suffer from high sky background, variable transmission and seeing, which explains why constructing even a small sample has been difficult. We describe our observations and reductions in Section 2 and our corrections for extinction and equivalent width measurements in Section 3. In Section 4, we perform statistical tests in an attempt to determine which properties affect dust grain-growth. In particular, we ask the questions (1) *Is grain growth correlated between binary pairs?* and (2) *Does removing this effect reveal correlations between grain growth and other properties?* We discuss the implications of our results and our conclusions in Section 5.

2. Observations and Reductions

We observed 7 T Tauri binaries with MMTAO/BLINC-MIRAC4 over several nights in 2009 and 2010 (the object names, dates, and exposure times can be found in Table 1). All of the objects were observed with the 6.5 meter MMT Telescope and its unique

²Taurus-Auriga is a low-mass star forming region with an age of $\sim 1-2$ Myr and a distance of ~ 140 pc (Kenyon & Hartmann 1995; Kenyon et al. 1994).

deformable-secondary adaptive optics system (MMTAO; Lloyd-Hart 2000; Wildi et al. 2003; Brusa et al. 2004), which produces stable, high-Strehl (up to $\sim 98\%$) point-spread-functions (PSFs) in the mid-infrared (Close et al. 2003). We used the combination mid-IR nulling-interferometer/imager/spectrograph, BLINC-MIRAC4 (Bracewell Infrared Nulling Cryostat; Mid-IR Array Camera, Gen. 4), in its imager/spectrograph configuration (Hoffmann et al. 1998; Hinz et al. 2000; Skemer et al. 2009).

For each binary, we observed a bright spectroscopic standard, that doubled as a PSF star, before and after the binary observation. We took acquisition images at $8.7\mu\text{m}$ to put the standard or binary in MIRAC4’s $1'' \times 15''$ slit. We then inserted the KRS-5 grism, which is in a filter wheel, near a pupil plane. For the binaries, we azimuthally aligned both stars with the slit, either based on our $8.7\mu\text{m}$ images or on optical acquisition images for the AO-system’s wavefront sensor. The telescope’s Cassegrain de-rotator was turned on to keep both stars in the slit. We chopped perpendicularly to the slit with an $8''$ throw, and nodded along the slit (so that the binary was visible in both nods) with $\sim 3\text{-}5''$ nods, depending on the binary separation.

The adaptive optics (AO) system is able to run at full-speed (550 Hz loop-speed) for stars brighter than $V \sim 12$ mag, and sometimes fainter in good conditions. Since some of our targets were fainter than this cutoff, we ran the AO system slower (100-150 Hz loop-speed) on these binaries, and their PSF star/spectroscopic standards. Our PSF/spectroscopic standard stars were brighter at visible wavelengths than our target binaries, so we used neutral density filters in the AO camera to roughly match the wavefront sensor counts and limit differences in photon-noise error.

Our reduction methods are described in Skemer et al. (2010). One difference is that in this paper, instead of having an overall “measurement error”, we often measure relative errors (between binary sources) separately from absolute errors (between one or both binary components and a spectroscopic standard). One benefit of this is that for sources with large (>2) mid-IR flux ratios, we can do an absolute calibration on just the brighter component with the best subset of our observations (i.e., close in airmass and time to bracketing spectroscopic standards and in photometric conditions), and build up S/N on the fainter companion in other conditions, without having to frequently switch between the object and a standard. The method is also useful for tight binaries, where we can use a subset of the data to do the absolute calibration on the combined binary, and then use the full dataset to split the binary. We use this method for all but GG Tau, and XZ Tau (2009 dataset), which were observed only briefly, so that all of the data were used for both relative and absolute calibrations. The exposure times for our absolute calibrations (a subset of our full data) and our relative calibrations (our full data) are listed in Table 1.

We used the mid-IR standard ϵ Tau for all of our binaries except GG Tau, for which we used HR 1684 (Cohen et al. 1999). In all cases except GG Tau and XZ Tau (2009 dataset), we were able to measure telluric calibration errors (as in Skemer et al. 2010) with bracketing standards. In the cases of GG Tau and XZ Tau (2009 dataset), which were both taken in photometric conditions with well-matched single spectroscopic standards in both airmass and time, we conservatively assume 3% local errors and 5% global flux errors outside of telluric ozone.

Most of the binaries in our survey have a large enough separation that splitting them is trivial with the 6.5 meter MMT and its adaptive optics system. However, a few of our binaries (GG Tau, GN Tau, XZ Tau, which are separated by 0.25", 0.41" and 0.29" respectively) are near or below the diffraction limit ($\lambda/D = 0.32''$ at $10\mu\text{m}$) of the 6.5 meter MMT. Because of MMTAO's high-Strehl and stability in the mid-infrared, it has resolved binaries as tight as 0.12" at $10\mu\text{m}$ using superresolution techniques (Skemer et al. 2008). By using our spectroscopic standard as a 1-D PSF, we fit a double (binary) PSF, for each wavelength of our spectrum image, fixing the separation of the binary based on imaging data. This gives us a measurement of the flux of each component relative to our spectroscopic standard.

For our tightest object, GG Tau, we also fixed the curvature of the grism trace to that of the PSF star's grism trace, which is legitimate as long as the object and PSF star are observed at a similar airmass to avoid the effects of atmospheric dispersion (Skemer et al. 2009). Both GG Tau and its PSF star were observed at 1.04 airmasses.

For GN Tau, the A and B components are of similar brightness in the optical, and because of their small separation, the AO system's wavefront sensor was somewhat less effective in the direction of the binary. As a result, the binaries' PSF was slightly wider in the direction of the binary than the spectroscopic standard's PSF. We found that convolving our spectroscopic standard's PSF with a $0.05''$ - σ Gaussian greatly improved the residuals of the binary fit, although this smoothing did not significantly affect the measurement values of the fit.

Spectrally dispersed images for each of our seven binaries are shown in Figure 1. Each frame shows both components of a binary, with the primary on top and the secondary on the bottom (primary being defined as the brighter component in the optical). A vertical cut through each image is shown to the right. Our tightest binaries, GG Tau Aa-Ab and XZ Tau A-B are separated by less than the MMT's $\sim 0.32''$ diffraction limit. However, the vertical cut through the spectrally dispersed images shows a wider spectrum, and with knowledge of the binary separation (obtained from acquisition images) and our high-Strehl ($\sim 98\%$) PSF, we are able to spatially resolve the spectra.

Spectroscopy for each of our seven binaries (plus a second epoch on one of the binaries, XZ Tau), is presented in Figure 2. In all cases, the A component is to the left and the B component is to the right. The error bars that coincide with the Earth’s 9.7 μm ozone feature reflect the larger calibration uncertainties of our data at these wavelengths.

A summary of all (our survey plus literature) spatially and N-band spectrally resolved binaries/multiples in the Taurus-Auriga star forming region is presented in Table 2. We rebin published spectra from other instruments (DD Tau A-B and FV Tau A-B from Honda et al. 2006 and GI-GK Tau from Watson et al. 2009) to the wavelength sampling used in our reductions in order to keep our results consistent. The uncertainties for DD Tau A-B and FV Tau A-B are from Honda et al. (2006). The uncertainties for GI-GK Tau are dominated by our binning method (see Skemer et al. 2010) because of *Spitzer*’s high sensitivity. Flux loss due to *Spitzer* slit mispointings become irrelevant in our later analysis of silicate equivalent widths.

3. Analysis

3.1. Correction for Extinction

Our mid-IR spectra must be corrected for extinction to avoid contamination by the silicate feature of the ISM extinction curve (Rieke & Lebofsky 1985). In Taurus, where most Class II objects are extinguished by $A_V < 3$ (Kenyon & Hartmann 1995), the effect is not as great as in other star forming regions. However, some of our objects have larger extinctions (the largest of which is FV Tau AB, with $A_V = 5.3$; White & Ghez 2001). As shown in Figure 1 of Furlan et al. (2009), these extinctions will have a strong influence on the resulting silicate emission feature if left uncorrected.

We correct for extinction in our measured mid-IR spectra using A_V values from Furlan et al. (2009) and references within (listed in Table 3), which will allow us to make a consistent comparison between our binaries and the single stars of Furlan et al. (2009) in Section 4.1. We adopt the same extinction laws as Furlan et al. (2009): Mathis (1990) with $R_V = 5$ for objects with $A_V < 3$ and McClure (2009) for $A_V \geq 3$. Since our objects are binaries, we correct extinction in both components equally, as interstellar extinction is thought to be the same between tight binary components (White & Ghez 2001; Hartigan & Kenyon 2003). The one exception is for our widest binary, GI-GK Tau, where Furlan et al. (2009) cite separate extinction values for each component.

Figure 3 shows our extinction corrected spectra. There are several examples of binaries that have strikingly similar silicate features, both in terms of their strengths and their shapes.

Notable examples include FX Tau, GN Tau, IT Tau, DD Tau, FV Tau and GI-GK Tau. We quantitatively compare the strength of silicate features in binary pairs, using equivalent width measurements, in Section 4.1. More detailed comparisons of their detailed silicate properties would be useful for determining whether individual dust components (for example, certain crystalline species) are correlated between binary pairs, but that test is not addressed further in this paper.

Our sample shows a diversity of silicate properties. Strong features (implying small dust grains) are present in GI Tau, GK Tau, RW Aur B and GG Tau Ab, among others. Weak features (no small grains) appear in IT Tau A and B and most notably in XZ Tau B, which shows negligible emission in 2009. XZ Tau, which was observed twice, shows strong variability, as was seen in multi-epoch *Spitzer* spectroscopy (Bary et al. 2009). Our data indicate that silicate variability is present in both sources, and because of the strong variation we observe in the flux ratio of the binary, both silicate features likely affect the unresolved *Spitzer* variability.

3.2. Equivalent Width Measurements: A Signature of Grain Growth

Numerous authors have noted the correlation between the shape and the strength of the 10 micron silicate feature, where a strong feature generally implies the presence of small grains. Since the ISM is composed of small, amorphous silicate grains (Kemper et al. 2004), it is assumed that circumstellar disks where these grains are observed have not undergone dust processing/grain growth, while disks with larger and/or more crystalline grains have begun grain growth. The 10 μm silicate feature is only sensitive to a subsample of dust in the circumstellar disk: silicate dust grains between $\sim 0.1\mu\text{m}$ and $\sim 5\mu\text{m}$, that are at the optically thin surface of the disk and at the proper temperature to be in the silicate emission zone (Kessler-Silacci et al. 2007). While the 10 μm silicate feature is being used to probe grain properties in the upper-layers of the circumstellar disk, millimeter wavelengths can probe the cooler and deeper layers of the disk, which contain larger mm-cm sized grains. The shape of the millimeter continuum slope can be used to probe a characteristic mid-plane grain size, which has also been used to infer grain-growth. In a highly important work, Lommen et al. (2010) demonstrated a correlation between the strength of the silicate feature (using equivalent width) and the slope of the millimeter continuum. This means that despite the limited emission zone of the 10 μm silicate feature, it does appear to be a marker for dust grain-growth throughout young circumstellar disks. This result has practical importance, because there are many more measurements of 10 μm silicate features than millimeter slopes, due to the decreasing brightness of these objects with wavelength. Binarity, in particular, is

best studied at shorter wavelengths where the system can be spatially resolved.

Lommen et al. (2010)’s result correlates the equivalent width of the silicate feature with dust grain sizes in the disk midplane. Similarly, silicate de-composition techniques (see Sargent et al. 2009; Juhász et al. 2009; Olofsson et al. 2010; Oliveira et al. 2011 and a review by Watson 2009) establish that the silicate feature equivalent width is connected to the size of dust grains in the upper layers of the disk. Based on these two correlations, we use the equivalent width of the silicate feature as a proxy for grain-growth for the rest of this paper. While silicate feature de-composition techniques still contain more information than this simple approach, equivalent width is a robust, single-number statistic, that is easily measured with ground-based systems that are limited in sensitivity, spectral range, and spectral resolution.

We calculate equivalent width by integrating $(F - F_{\text{continuum}})/F_{\text{continuum}}$, where the continuum is a linear fit of our flux measurements between 8.07-8.27 μm and 12.56-12.95 μm . Errors are calculated using the Monte Carlo approach described in Skemer et al. (2010). The dominant error source for most of our MMTAO/BLINC-MIRAC4 data is the spectroscopy at the edges of the silicate band, which define the (linear-fit) silicate continuum. These regions are particularly faint from the ground because of the low atmospheric transmission $\leq 8\mu\text{m}$ and $\geq 12.5\mu\text{m}$ combined with decreasing flux at the longer wavelengths. The other difficult region in the N-band is the 9.7 μm telluric ozone feature, where our absolute calibrations tend to be much worse than elsewhere in the spectrum (see Figure 2). For the purposes of calculating equivalent width, we interpolate over the ozone region.

The results of our equivalent width measurements of binaries, as well as 8.1 and 12.7 μm continuum photometry and colors are presented in Table 3. We include our MMTAO/BLINC-MIRAC4 measurements, as well as the binaries from Honda et al. (2006) and Watson et al. (2009), which we interpolate in the same fashion as the MMTAO/BLINC-MIRAC4 for consistency. We do not include T Tau, UY Aur or XZ Tau, which are not used in Section 4.1 because they are self-extincted and variable. All of the quantities listed are calculated with the extinction corrected spectra.

Our ground-based equivalent width measurements use a smaller than desirable wavelength range ($\sim 8\text{-}12.5\mu\text{m}$) due to truncation by atmospheric transmission. Space-based equivalent width measurements, motivated by the true width of the silicate feature, use larger wavelength ranges (for example, Lommen et al. (2010) use 7.5-13.0 μm). Additionally, space-based equivalent width measurements often use polynomial continuum fits instead of linear fits and do not interpolate over telluric ozone, as is done for our ground-based measurements. For these reasons, it is worth checking that the equivalent widths calculated using our ground-based prescription are well-correlated with the equivalent widths calculated us-

ing typical space-based prescriptions. We use a set of single stars in Taurus (described in Section 4.1), whose extinction corrected equivalent widths are published by Furlan et al. (2009) based on *Spitzer*/IRS spectroscopy. We obtained the *Spitzer* data, and applied our MIRAC4 binning procedure and equivalent width measurements prescription. A comparison of our measurements with the measurements of Furlan et al. (2009) is shown in Figure 4. The space-based prescription (true) equivalent widths are well-correlated with the ground-based prescription (truncated) equivalent widths, with the exception of one outlier (DM Tau, which has a large quadratic continuum term (Watson et al. 2009) that is not accounted for in the ground-based prescription). This implies that ground-based (truncated) equivalent widths are reliable proxies for the space-based (true) equivalent widths.

4. Statistical Tests

4.1. Is Grain Growth in Binaries Correlated?

Properties shared between binary stars, such as age, composition and formation history, might be linked to the growth of dust grains in young stars. We test for this by determining if the silicate features of binary stars are more similar than the silicate features of randomly selected pairs of single stars. We use the ratio of extinction corrected equivalent width measurements (Table 3) to quantify the similarity of two silicate features, using the reciprocal of the ratio when the ratio is < 1 .

The binary stars are drawn from our sample of spatially and spectrally resolved N-band spectra in Taurus-Auriga (Table 2), where we exclude systems that contain infrared companions, that are thought to be self-extincted and variable (T Tau, UY Aur, XZ Tau, as shown by van Boekel et al. 2010; Skemer et al. 2010; Bary et al. 2009). This leaves us with 9 binaries for the test. For the pairs of single stars, we use the extinction corrected equivalent widths of 26 Taurus-Aurigae single stars from Furlan et al. (2009), where the single stars are listed in Furlan et al. (2006). We exclude sources with unknown and high ($A_V > 8$) extinctions, and we avoid DG Tau, which is known to have a variable silicate feature (Wooden et al. 2000; Bary et al. 2009) and HK Tau, which has a self-extincting disk (Stapelfeldt et al. 1998). We recalculate the extinction-corrected equivalent widths of the single stars using our ground-based prescription (see Section 3.2) and list these values in Table 4. The single stars and binaries are similarly distributed on an HR diagram (Figure 5), allowing us to make a reasonably unbiased comparison.

We do an $N=10^4$ Monte Carlo simulation to randomly pair single stars and to randomly sample the error bars for our binary equivalent width ratios (a histogram of the simulation

output is shown in Figure 6. In 90% of our trials, the average (mean) of the equivalent width ratios of the 9 binaries is closer to 1 than the average equivalent width ratios of 9 randomly selected pairs of single stars. Thus, with 90% confidence, we find that silicate features in binary pairs are more similar than silicate features in randomly paired single stars, implying that grain growth is correlated in binaries.

There is one systematic effect that is likely to have increased the observed differences between the silicate features of the single star pairs. The extinction measurements for each single star correspond to an approximately 15% error in equivalent width (Furlan et al. 2009). This will cause a residual differential extinction between the single star pairs, that should on average make the single star silicate features look more different than they actually are. We add 15% more uncertainty to the single star equivalent widths in our Monte Carlo simulation and find that our confidence is only changed by 2%. Thus, the effect of residual extinction in the single star pairs is small. Similarly the extinction corrections for the binaries, described in Section 3.1, assumes that the binaries share the same interstellar extinction. If this assumption is incorrect there would be a residual differential extinction between the binary pairs, that should on average make the binary silicate features look more different than they actually are. This bias is similarly small to the single star bias.

Our single star sample includes 3 transition disks (GM Aur, DM Tau and LkCa 15), which have larger than normal silicate equivalent widths (see Figure 4 and Furlan et al. 2009). We include them in our single star sample because some of our binaries have similarly large silicate equivalent widths (for example GG Tau Ab, which has a “truncated” $EqW = 3.33 \pm 0.40$). Excluding the transition disks (while including GG Tau) would change our confidence that grain growth is correlated in binaries to 83%.

Of our 9 binaries, GG Tau Aa-Ab has the largest disparity between its silicate feature equivalent widths. GG Tau A is a 0.25” binary with circumstellar disks around each component and a spatially resolved circumbinary disk (Dutrey et al. 1994) that is unusually massive (Jensen et al. 1996). Some authors have reported tentative detections of a dust streamer onto GG Tau Ab (Roddier et al. 1996; Piétu et al. 2011), which might be replenishing the small dust grains detected in our silicate spectroscopy (Skemer et al. 2010). The presence of streamers has also been inferred in tighter binary systems via periodic accretion (Mathieu et al. 1997; Jensen et al. 2007). If the dust steamer(s) replace the dust grains around each components at different rates, the silicate features would not be “coeval” as we have assumed throughout this analysis. Excluding GG Tau (and the transition disks) from our Monte Carlo simulation would change our confidence that grain growth is correlated in binaries to 95%.

4.2. Does the Coevality of Binaries Reveal a Correlation of Grain Growth and other Properties?

Numerous authors have used single stars (and unresolved binaries) to determine if stellar and disk properties might correlate with grain-growth. The strongest correlation is between X-ray luminosity and dust grain crystallinity and size (Glauser et al. 2009; Riaz 2009). A weaker and possibly dependent correlation might exist between stellar mass and dust-grain size (Kessler-Silacci et al. 2006; Pascucci et al. 2009). It is possible that age and/or formation history effects are obscuring the correlations between grain growth and stellar/disk properties. Here, we use the coevality of binaries to effectively remove the age/formation history affects and test correlations between grain-growth and various other parameters.

As in Section 4.1, we use the 9 binaries from our sample that do not have edge-on disks/self-extinction. For each of these binaries, we have compiled a table of spatially resolved ancillary stellar properties (Table 5) and a table of infrared flux ratios for determining disk colors (Table 6). We plot 6 different stellar/disk properties versus binary equivalent width ratios in Figure 7. With our small sample size of binaries (9), doing too many correlation tests would result in spurious correlation detections. Thus, the properties we have chosen are intended to have the most plausible links to grain-growth. Spectral type is an obvious catch-all, that for a fixed age, is related to the temperature, luminosity and mass of the star. Bolometric magnitude relates to the total flux hitting the dust-grains, and should define the “silicate emission zone” (Kessler-Silacci et al. 2007). Stellar mass relates to the gravity-induced sinking of large dust grains to the disk midplane and disk dynamics in general. H_α relates to accretion, which will produce UV photons that can anneal the dust. K-L colors relate to the geometry of the disk’s puffed-up inner-rim. K-N colors relate to the disk geometry at the location of the silicate emission zone.

For each frame in Figure 7, the x-axis shows a difference/ratio measurement for a star/disk property. For example, frame (a) shows the difference in spectral type between the A component and the B component of the binary. In all frames, the y-axis shows the ratio of the equivalent width ratios. Vertical dotted lines show equal spectral types, luminosities, masses, H_α equivalent widths, and colors. Horizontal dotted lines show equal silicate equivalent widths. This divides each frame into quadrants. We do a coarse correlation analysis by determining how many binaries are in the top-right or bottom-left quadrants versus the top-left or bottom-right quadrants. This allows us to easily answer questions of the form “Do the stars with earlier spectral types have larger or smaller silicate feature equivalent width?” Since we are dealing with coeval binary pairs, this directly relates to whether spectral type is correlated with grain-growth.

In 7 out of 9 binaries, the star with the earlier spectral type has a smaller silicate equiv-

alent width than the star with the later spectral type. Using the binomial distribution with $p = 50\%$, the probability that 7 or more out of 9 binaries would have larger equivalent widths in either the earlier-type components or the later-type components is 18%. This probability is not low enough to rule out the null hypothesis that spectral type is not correlated with silicate feature equivalent widths (especially given that it is 1 of 6 tests shown in Figure 7). No other parameter in Figure 7 has a stronger correlation signal than spectral type. Additionally, none of the parameters in Figure 7 have an obvious visual trend. Thus, we do not find evidence for any correlations with equivalent width, other than the marginal one observed for spectral type.

5. Discussion and Conclusions

Our mid-infrared adaptive optics survey has produced 8 new spatially resolved silicate spectra of young Taurus-Aurigae binaries (including UY Aur, which was published in Skemer et al. 2010). This effectively triples the number of spatially and spectrally resolved binaries in the Taurus-Auriga cluster, and provides the first opportunity to draw statistical conclusions about the spatially resolved silicate features of binaries in any young cluster. Our fundamental questions are (1) *Is grain growth correlated between binary pairs?* and (2) *Does removing this effect reveal correlations between grain growth and other properties?*

We find with 90% confidence (when including GG Tau) or 95% confidence (when excluding GG Tau) that the silicate features of binaries are more similar than the silicate features of randomly paired single stars (our ambivalence in including GG Tau stems from its large circumbinary disk, which might be replenishing the dust in the inner disks via streamers). The similarity of the silicate features in our binary pairs implies that one or more shared binary properties (such as age, composition or formation history) plays an important role in dust grain evolution.

One possible explanation for our findings is that the environment in which a star forms affects its potential to grow dust grains, and eventually planets. It is a fundamental prediction of core-accretion that giant planets form more efficiently in metal-rich systems, based on the increased solid material available for building planetary cores (Ida & Lin 2004a,b). However, the core-accretion scenario is predicated by small dust grains coagulating quickly enough that aerodynamic drag does not remove too many meter-sized objects from the system (a problem, which is commonly known as the “meter-sized barrier”; Weidenschilling 1977). Brauer et al. (2008) have shown that the removal of meter-sized objects due to radial drift can be overcome by increasing the disk’s initial dust-to-gas ratio from 1% to 2%. The result is a natural consequence of increasing the rate of grain growth by decreasing the time

between collisions. Since binary stars form from the same fragmented core material, it is possible that grain growth in binary stars will proceed at similar rates in each component due to their shared initial gas-to-dust ratio.

Binarity itself might also affect the silicate features of young stars. Circumstellar disks can be dynamically perturbed by a companion star, which introduces spiral structure and truncates the radial extent of the disk (Artymowicz & Lubow 1994). In this configuration, large particles collide and fragment more frequently, which speeds up dust grain evolution (Dubrulle et al. 1995) while decreasing the maximum particle size in the disk (Zsom et al. 2011). Dust streamers from a wider circumbinary disk can also replenish solid material in one or both of the circumstellar disks (Artymowicz & Lubow 1996). The dust streamers are likely to contain un-evolved, ISM-like dust grains that dominate the appearance of the silicate feature (Skemer et al. 2010). There are two young Taurus-Aurigae binaries with directly imaged circumbinary disks: GG Tau (Dutrey et al. 1994) and UY Aur (Dutrey et al. 1996). In each case, we find that one of the components has an unusually prominent silicate feature, indicating the presence of small grains. Pascucci et al. (2008) were not able to detect a difference between the silicate features of (unresolved) medium-separation binaries and single stars, which suggests that any effect must be subtle or uncommon. However, spatially resolved studies of the silicate features in young binaries might reveal different dust-grain growth mechanisms.

In Section 4.2, we found that seven of our nine binaries (i.e. 82% confidence of a trend using the binomial distribution) have larger silicate equivalent widths (smaller grains) in the secondary than the primary. This pattern was also observed in two binaries by Przygodda et al. (2003). Assuming this trend is confirmed by larger samples of spatially resolved silicate spectroscopy, the cause could be based on the dynamics of binaries or simply a spectral-type/mass/luminosity correlation with the speed of dust grain growth. The former explanation could be tested by seeing if the correlation is connected with binary separation.

Our study has been limited by its small sample size, due to the complexity and limitations of ground-based 10 μm spectroscopy and adaptive optics, which were necessary to build up the current sample. Larger ground-based telescopes, such as the LBT and ELTs along with large space-based telescopes, such as JWST will be able to dramatically increase the sample of spatially resolved silicate spectra of young binaries.

The authors thank Elise Furlan, Mitsuhiko Honda and Dan Watson for providing us with their published spectra. We also thank Daniel Apai, Ilaria Pascucci and Kevin Flaherty for useful discussions regarding grain-growth and silicate variability. AJS acknowledges the NASA Graduate Student Research Program (GSRP) for its generous support of this project.

We also thank the MMT staff, especially Mike Alegria, Morag Hastie and Ricardo Ortiz for operating the AO system during a difficult set of observations.

Table 1. MMTAO/BLINC-MIRAC4 Observations of T Tauri Binaries

Binary	Dates (UT)	Relative Calibration On-source Time (s) ^a	Absolute Calibration On-source Time (s) ^a
DK Tau	2010 Jan 3	2190	1260
FX Tau	2010 Jan 2 and 6	1200	570
GG Tau A	2009 Oct 2	1200	1200
GN Tau	2010 Jan 2	2550	750
IT Tau	2010 Jan 3 and 4	2385	2385
RW Aur	2010 Jan 5 and 6	765	630
XZ Tau	2009 Jan 14	160	160
XZ Tau	2010 Jan 5	1230	270

^aRelative fluxes between binary pairs were measured using all available data. Absolute calibrations (using the brighter star or the “un-resolved” binary pair) were measured using the best subset of data to minimize errors caused by changing atmospheric conditions.

Table 2. N-band Spatially and Spectrally Resolved Taurus Binaries

Binary	Separation (")	Separation Ref.	N-band spectra Ref.
DD Tau A-B	0.56	1	2
DK Tau A-B	2.32	1	this work
FV Tau A-B ^a	0.71	1	2
FX Tau A-B	0.89	1	this work
GG Tau Aa-Ab ^b	0.25	this work	this work
GI-GK Tau ^c	12.9	3	4
GN Tau A-B	0.41	this work	this work
IT Tau A-B	2.4	5	this work
RW Aur A-B ^d	1.40	1	this work
T Tau N-Sa-Sb	0.69/0.13	6	7
UY Aur A-B	0.88	1	8
XZ Tau A-B ^e	0.29	this work	this work

Note. — A list of T Tauri binaries in the Taurus-Auriga star-forming regions with spatially resolved N-band spectroscopy. We only include binaries separated by $< 30''$, which are then likely to be bound and coeval (Kraus & Hillenbrand 2009). Due to non-negligible orbital motion in the cases of GG Tau, GN Tau and XZ Tau, astrometry is measured from $8.7\mu\text{m}$ acquisition images preceding our N-band spectroscopy. We use α Gemini as our astrometric standard. T Tau Sa-Sb also has fast orbital motion, which is parameterized, most recently, by Köhler et al. (2008)

^adoes not include FV Tau /c, which is a $0.7''$ binary located $12.3''$ from FV Tau (White & Ghez 2001)

^bdoes not include GG Tau B, which is a $0.25''$ binary located $10.3''$ from GG Tau A (White & Ghez 2001)

^cGK Tau is itself a $2.4''$ binary (Hartigan et al. 1994). However, GK Tau B was not detected in our 8.7 micron imaging.

^dRW Aur was found to be a triple by (Ghez et al. 1993), but (White & Ghez 2001) claim the 3rd star was probably a false detection.

^eXZ Tau A is itself a $0.09''$ binary at mm wavelengths (Carrasco-González et al. 2009).

References. — (1) White & Ghez (2001); (2) Honda et al. (2006); (3) Hartigan et al. (1994); (4) Furlan et al. (2006), Watson et al. (2009) and others; (5) Duchêne et al. (1999); (6) Köhler et al. (2008); (7) Ratzka et al. (2009); (8) Skemer et al. (2010)

Table 3. Extinction Corrected Silicate/Continuum Measurements of T Tauri Binaries

	$A_V(mag)^a$	Silicate EqW (μm)	8.1 μm^b flux (Jy)	12.7 μm^c flux (Jy)
DD Tau A	1.0	0.95±0.06	0.45±0.01	0.73±0.00
DD Tau B	1.0	1.53±0.11	0.34±0.01	0.43±0.01
DD Tau A/B		0.62±0.06	1.33±0.06	1.72±0.03
DK Tau A	1.3	2.80±0.18	0.66±0.03	0.78±0.02
DK Tau B	1.3	1.76±0.25	0.15±0.01	0.14±0.01
DK Tau A/B		1.60±0.18	4.51±0.14	5.52±0.30
FV Tau A	5.3	1.03±0.10	0.30±0.00	0.32±0.01
FV Tau B	5.3	1.44±0.11	0.43±0.01	0.54±0.01
FV Tau A/B		0.72±0.09	0.70±0.03	0.59±0.02
FX Tau A	2.0	2.61±0.39	0.14±0.01	0.17±0.02
FX Tau B	2.0	2.34±0.43	0.05±0.00	0.07±0.01
FX Tau A/B		1.12±0.26	2.91±0.22	2.45±0.35
GG Tau Aa	1.0	0.91±0.25	0.36±0.02	0.39±0.04
GG Tau Ab	1.0	3.33±0.40	0.24±0.02	0.28±0.02
GG Tau Aa/Ab		0.27±0.08	1.47±0.10	1.38±0.14
GI Tau	2.3	1.93±0.05	0.68±0.01	0.79±0.00
GK Tau	1.1	2.76±0.09	0.69±0.02	0.86±0.00
GI Tau/GK Tau		0.70±0.03	0.99±0.03	0.92±0.00
GN Tau A	3.5	1.04±0.21	0.14±0.01	0.15±0.01
GN Tau B	3.5	1.66±0.20	0.23±0.01	0.21±0.01
GN Tau A/B		0.62±0.12	0.59±0.03	0.75±0.04
IT Tau A	3.8	0.86±0.18	0.20±0.01	0.17±0.01
IT Tau B	3.8	1.06±0.37	0.08±0.00	0.07±0.01
IT Tau A/B		0.81±0.26	2.51±0.07	2.29±0.27
RW Aur A	0.5	1.10±0.07	1.05±0.05	1.26±0.05
RW Aur B	0.5	2.45±0.48	0.12±0.01	0.11±0.01
RW Aur A/B		0.45±0.10	8.43±0.62	11.81±1.59

Note. — All error bars are calculated by taking the interquartile range of our Monte Carlo simulation, and dividing by 1.34. This is a robust estimate of a Gaussian sigma.

^a A_V values from Furlan et al. (2009)

^bFlux measured between 8.07 μm and 8.27 μm

^cFlux measured between 12.56 μm and 12.95 μm

Table 4. Single Stars Used in Comparison with Binary Stars

	$A_V(mag)^a$	Spectral Type ^a	Silicate EqW (μm) ^b
04108+2910	1.4	M0	0.21
AA Tau	1.8	K7	1.18
BP Tau	1.0	K7	1.89
CI Tau	2.0	K7	1.61
CW Tau	2.8	K3	0.69
CX Tau	1.3	M0	1.05
CY Tau	1.7	K7	0.42
DE Tau	1.2	M0	1.21
DL Tau	1.5	K7	0.40
DM Tau	0.7	M1	1.43
DN Tau	0.6	M0	0.51
DO Tau	2.0	M0	0.65
DP Tau	0.6	M0.5	1.06
DR Tau	1.2	...	0.80
DS Tau	1.1	K5	1.66
F04147+2822	2.5	M4	1.75
FN Tau	1.4	M5	1.25
GM Aur	1.2	K3	3.50
GO Tau	2.0	M0	1.49
HP Tau	2.8	K3	1.69
IP Tau	0.5	M0	2.63
IQ Tau	1.4	M0.5	1.26
LkCa 15	1.2	K5	3.98
RY Tau	2.2	G1	4.02
V410 Anon 13	5.8	M6	0.99
V836 Tau	1.1	K7	2.02

^a A_V values and spectral types from Furlan et al. (2009)

^bEquivalent Widths are based on *Spitzer* spectra from Furlan et al. (2009) and are calculated using our ground-based prescription as described in Section 3.1

Table 5. Ancillary Stellar Properties of Taurus Binaries

Binary	Spectral Type	H_α EqW (\AA)	Ref.	M_{bol} (mag) ^a	M_{star}/M_\odot ^a
DD Tau A	M3.5	206	1	5.08	$0.43^{+0.13}_{-0.23}$
DD Tau B	M3.5	635		5.40	$0.41^{+0.11}_{-0.19}$
DK Tau A	K9	31	2	3.66	$0.71^{+0.09}_{-0.06}$
DK Tau B	M1	118		5.35	$0.61^{+0.06}_{-0.04}$
FV Tau A	K5	15	3,1		
FV Tau B	K6 ^b	63			
FX Tau A	M1	13	4	4.91	$0.62^{+0.05}_{-0.03}$
FX Tau B	M4	1.0		5.97	$0.28^{+0.16}_{-0.32}$
GG Tau Aa	M0	57	1,3 ^c	4.50	$0.73^{+0.09}_{-0.08}$
GG Tau Ab	M2	16		4.87	$0.64^{+0.03}_{-0.03}$
GI Tau	K6	20	5,6		
GK Tau	K7	22			
GN Tau A	M2.5 (unresolved) ^d	59 (unresolved)	7		
GN Tau B					
IT Tau A	K3	21.7	4	3.84	$1.0^{+0.3}_{-0.1}$
IT Tau B	M4	147		5.98	$0.28^{+0.15}_{-0.32}$
RW Aur A	K1	76	3	3.11	$1.4^{+0.6}_{-0.7}$
RW Aur B	K5	43		5.01	$0.86^{+0.11}_{-0.10}$

^a M_{bol} and M_{star} are calculated by Kraus & Hillenbrand (2009)

^bNote that Hartigan & Kenyon (2003) found no photospheric absorption lines in their STIS spectrum of FV Tau B.

^cHartigan & Kenyon (2003)’s GG Tau spectrum is saturated at H_α , so we use H_α equivalent width measurements from White & Ghez (2001).

^dAlthough GN Tau does not have a published resolved spectral type, it has been resolved in the optical (Simon et al. 1996), near-infrared (White & Ghez 2001) and mid-infrared (this work). Throughout this range of wavelengths, it has a near equal flux ratio, so it is likely that the binary consists of two nearly equal mass stars.

References. — (1) Hartigan & Kenyon (2003); (2) Monin et al. (1998); (3) White & Ghez (2001); (4) Duchêne et al. (1999); (5) Kenyon & Hartmann (1995); (6) Hartigan et al. (1994); (7) White & Basri (2003)

Table 6. Flux Ratios of Taurus Binaries

Binary	K Flux Ratio	L Flux Ratio	Near-IR Ref.	12.7 μ m Flux Ratio
DD Tau A-B	1.17 \pm 0.06	1.72 \pm 0.13	1	1.72 \pm 0.03
DK Tau A-B	4.21 \pm 0.30	4.02 \pm 0.13	1	5.52 \pm 0.30
FV Tau A-B	1.49 \pm 0.01	0.69 \pm 0.02	1	0.59 \pm 0.02
FX Tau A-B	2.20 \pm 0.02	2.97 \pm 0.03	1	2.45 \pm 0.35
GG Tau Aa-Ab	1.95 \pm 0.16	2.23 \pm 0.01	1	1.38 \pm 0.14
GI-GK Tau ^a	0.77 \pm 0.03	0.77 \pm 0.07	2,3	0.92 \pm 0.00
GN Tau A-B	1.17 \pm 0.03	1.25 \pm 0.03	1	0.75 \pm 0.04
IT Tau A-B	6.37 \pm 0.76	16.0 \pm 4.4	1	2.29 \pm 0.27
RW Aur A-B	4.23 \pm 0.16	6.16 \pm 0.24	1	11.81 \pm 1.59

^aPhotometry for GI Tau and GK Tau have been extinction corrected individually using the A_V values listed in Table 3.

References. — (1) White & Ghez (2001); (2) Skrutskie et al. (2006); (3) Luhman et al. (2006)

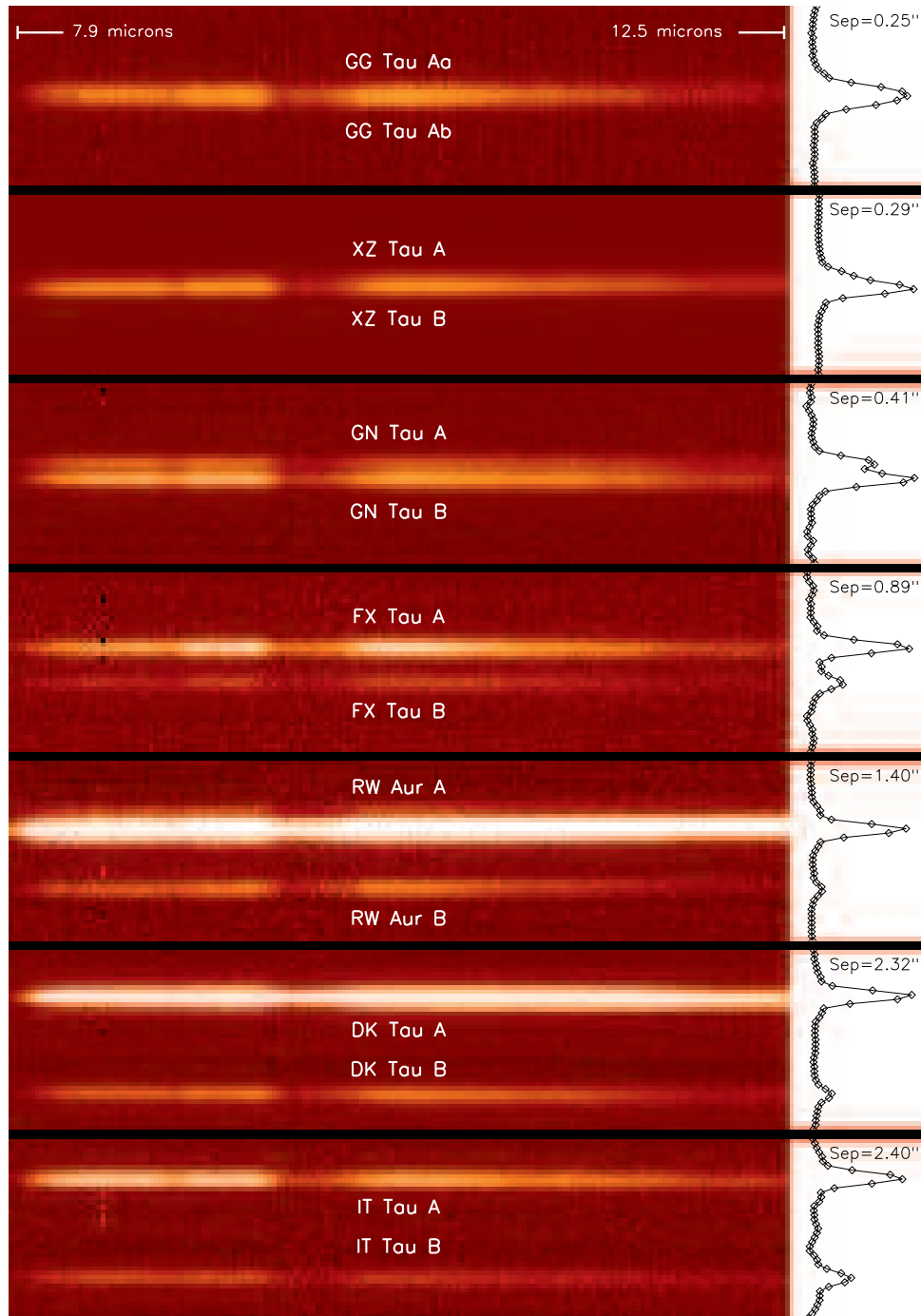


Fig. 1.— Spectrally dispersed images of 7 T Tauri binaries that we have spatially and spectrally resolved for the first time at N-band. The wavelength range (shown at the top) is $7.9\mu\text{m}$ to $12.5\mu\text{m}$ and has a suppressed flux at $9.7\mu\text{m}$ due to telluric ozone. The images are each $4.4''$ in the spatial direction and are displayed with (different) linear stretches. At the right of every spectrally dispersed image is a vertical (spatial direction) profile cut. GG Tau and XZ Tau are separated by less than the diffraction-limit of the 6.5 meter MMT but are superresolved due to the excellent stability of the MMT’s adaptive optics PSF in the mid-infrared. This is evident in the vertical profiles, which show that that GG Tau and XZ Tau are wider than the PSF (seen in the well-separated binaries below).

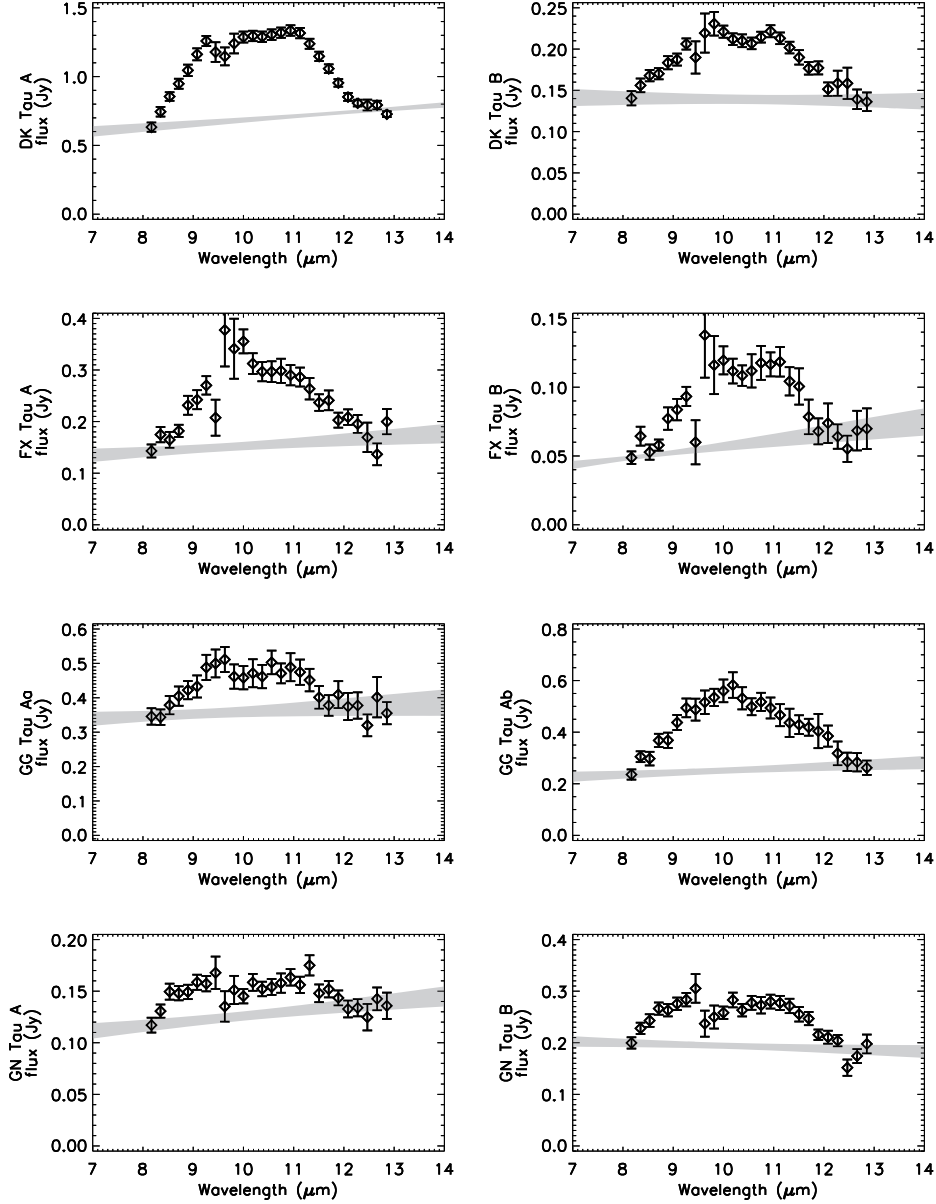


Fig. 2.— Spectra of 7 T Tauri binaries that we have spatially and spectrally resolved for the first time at N-band. XZ Tau is shown twice because we observed it once in 2009 and once in 2010. In all cases, the primary is shown on the left and the secondary is shown on the right. The grey region on each plot shows the 1σ range of our continuum fit, which we use when calculating equivalent widths. *Continued*

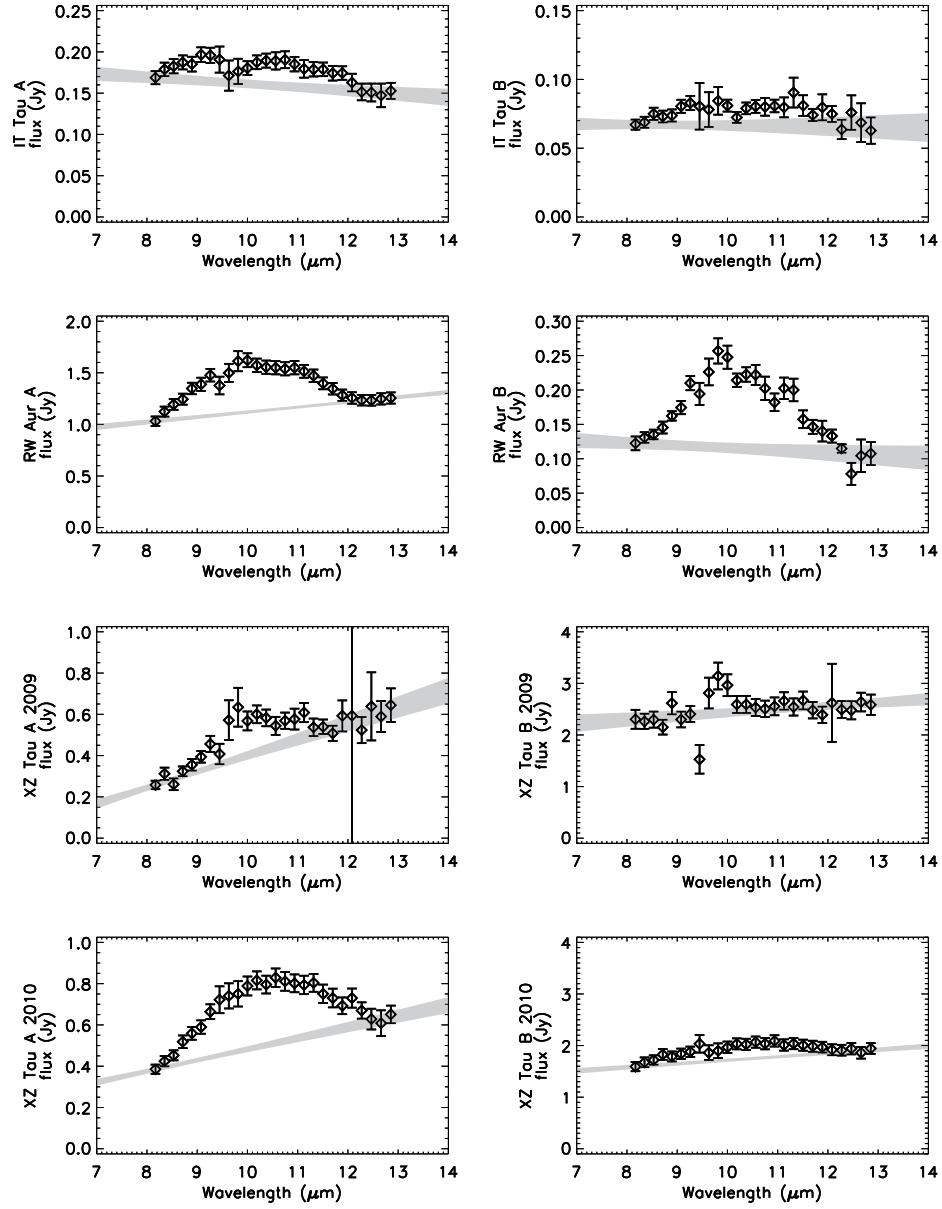


Fig. 2.— *Continued*

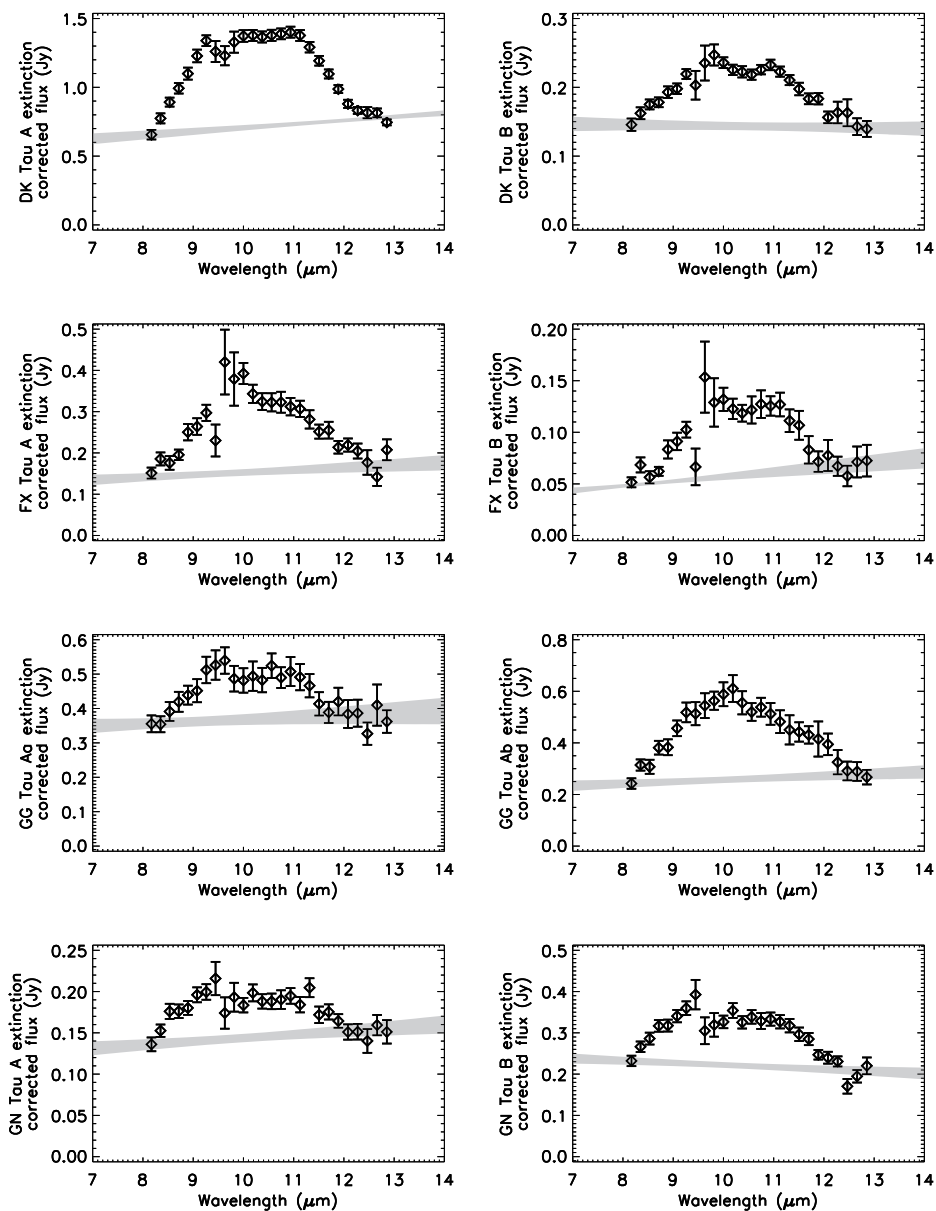


Fig. 3.— Extinction corrected spectra from Figure 2 with 3 additional binaries from Honda et al. (2006) and Watson et al. (2009). *Continued*

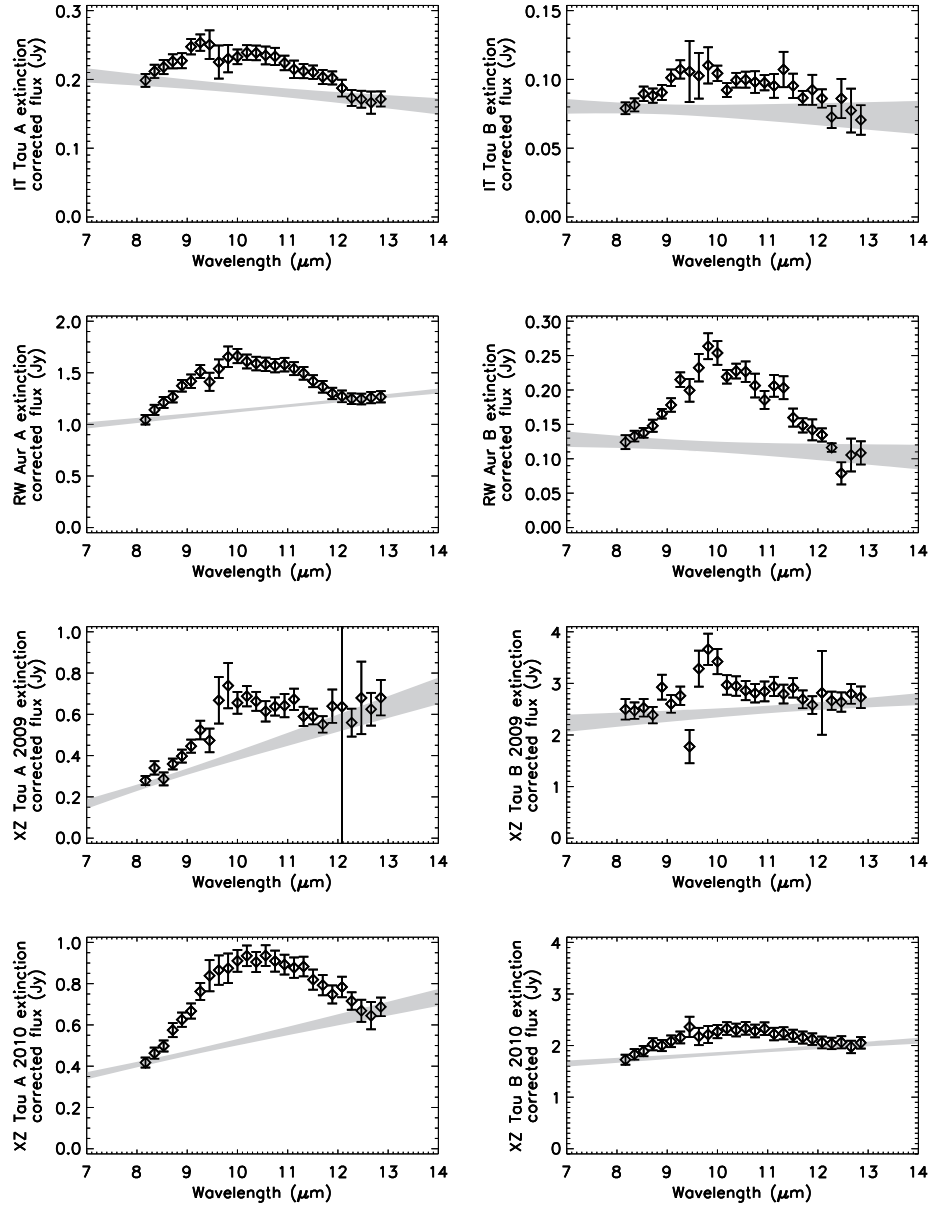


Fig. 3.— *Continued*

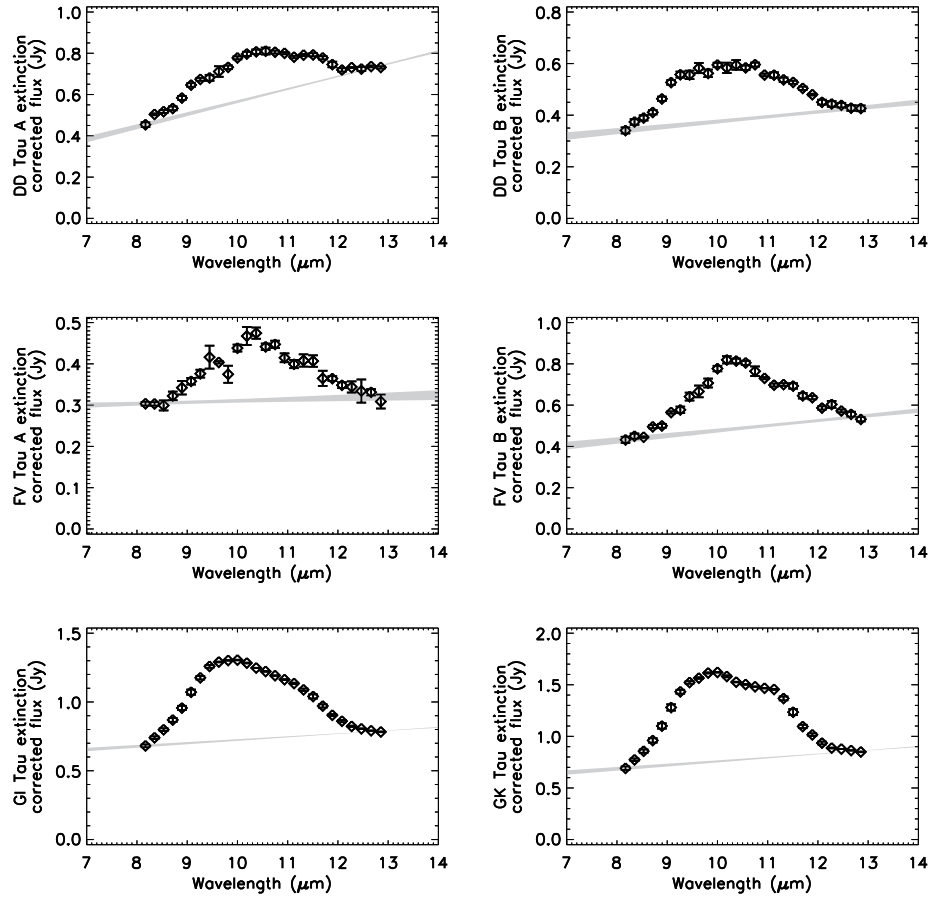


Fig. 3.— *Continued*

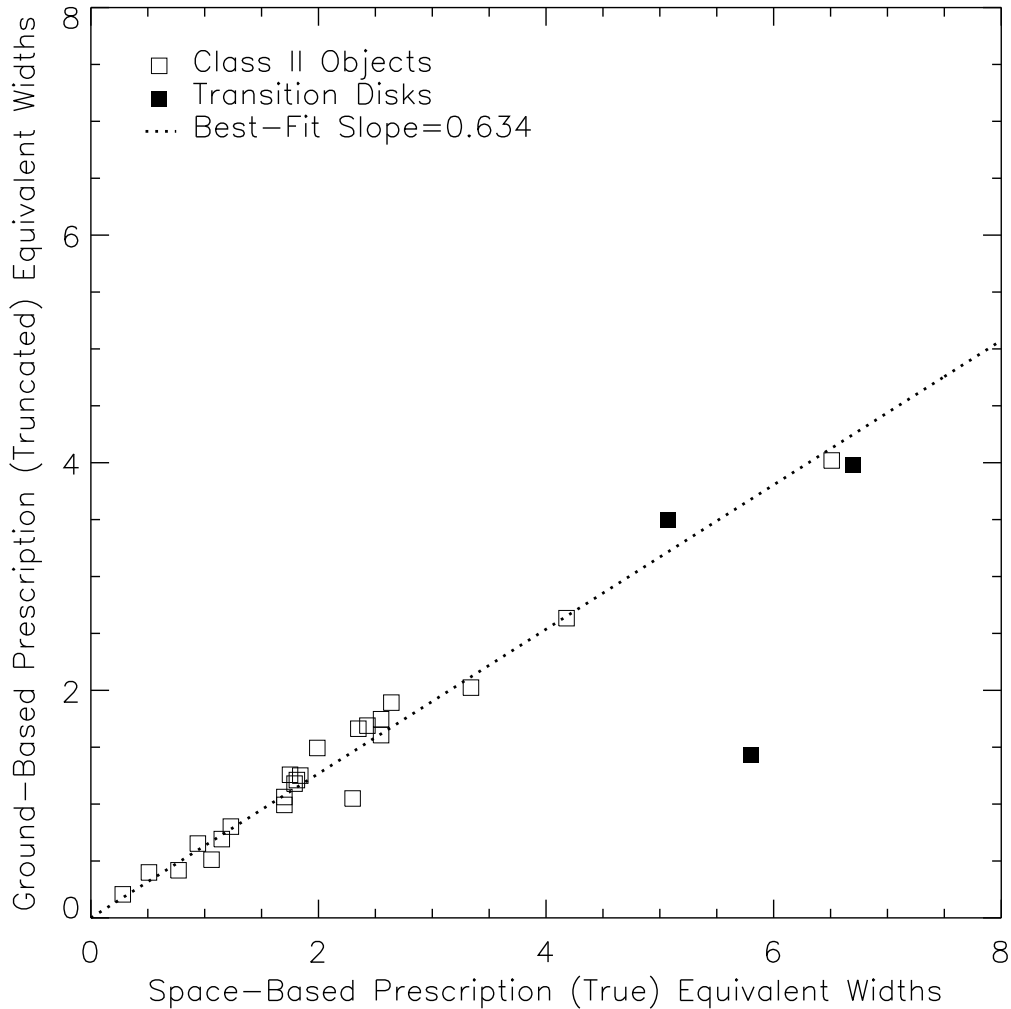


Fig. 4.— We take space-based equivalent width measurements from (Furlan et al. 2009) and compare them with equivalent width using the same data but a different (i.e., ground-based) measurement prescription. The different prescriptions produce well-correlated equivalent widths (as shown by the best-fit, dotted line), where the ground-based (truncated) equivalent widths are systematically lower by 36.6%. This means that ground-based (truncated) equivalent width measurements can be used as a proxy for space-based (true) equivalent-width measurements. Note that our plot has one outlier, DM Tau, due to the large quadratic term in its continuum that is not included in our ground-based prescription. The 3 transition disk objects all have unusually large equivalent widths.

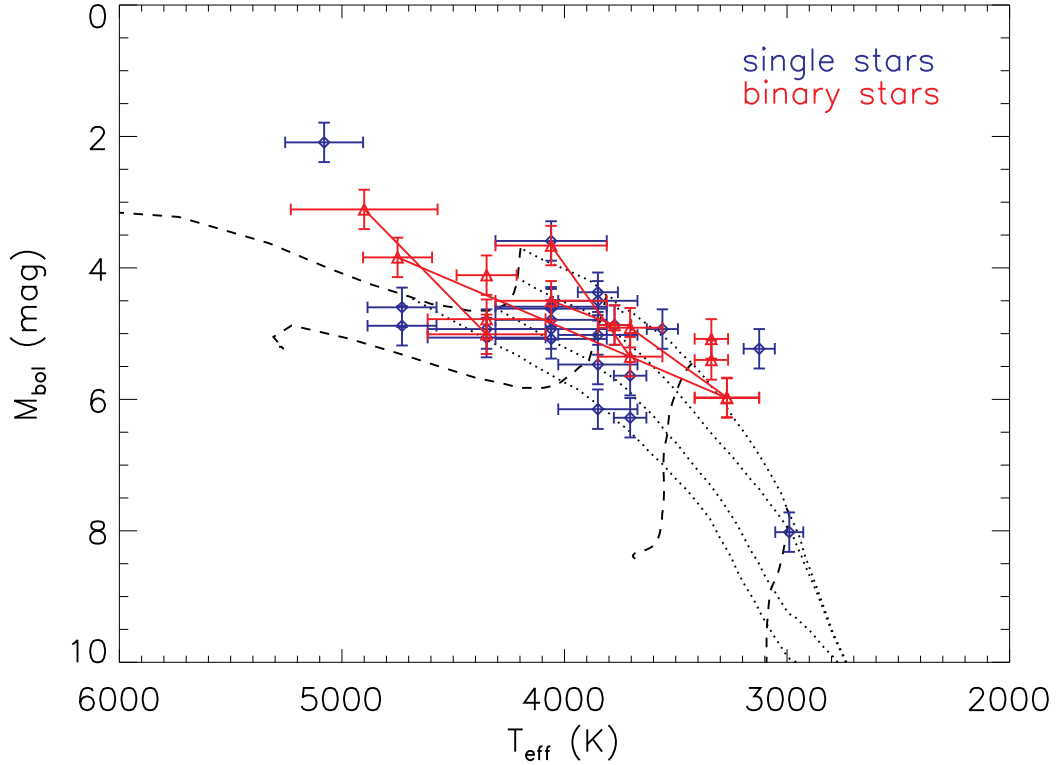


Fig. 5.— An HR diagram showing the similar distribution of single stars (blue diamonds) and binary stars (red triangles) used in our comparison of silicate features (Section 4.1). Binary pairs are connected with red lines when both stars are shown. T_{eff} and M_{bol} values are from Kraus & Hillenbrand (2009) when available (22 of 26 single stars and 14 of 18 stars in binaries). Isochrones (dotted lines; 1, 2, 5 and 10 Myr) and evolutionary models (dashed lines; 0.1, 0.5, 1.0 and 1.4 M_{\odot}) are from Baraffe et al. (1998). There is a noticeable spread in the ages and masses of our sources and not all of the binary pairs fall on the same isochrones. Some of this might be due to observations uncertainties or model errors. In aggregate, Kraus & Hillenbrand (2009) find that Taurus binaries are more coeval than random pairs.

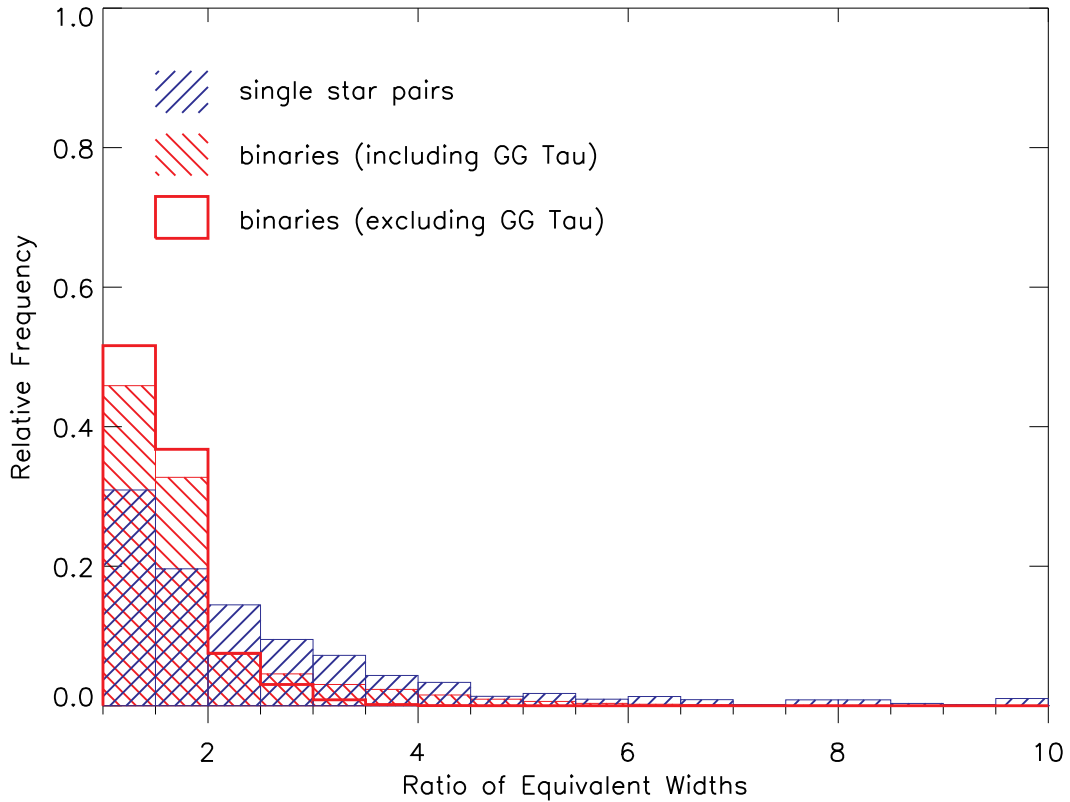


Fig. 6.— A comparison of equivalent width ratios from our binary sample and a sample of randomly paired single stars. Ratios close to 1 indicate that the silicate feature equivalent widths (which are a proxy for dust grain sizes) of a pair are similar. When including GG Tau Aa-Ab, which might have contaminated silicate features due to accretion from circumbinary streamers, we find with 90% confidence that the binary stars have more similar equivalent width ratios than randomly paired single stars. When excluding GG Tau Aa-Ab, we find with 95% confidence that the binary stars have more similar equivalent width ratios than randomly paired single stars.

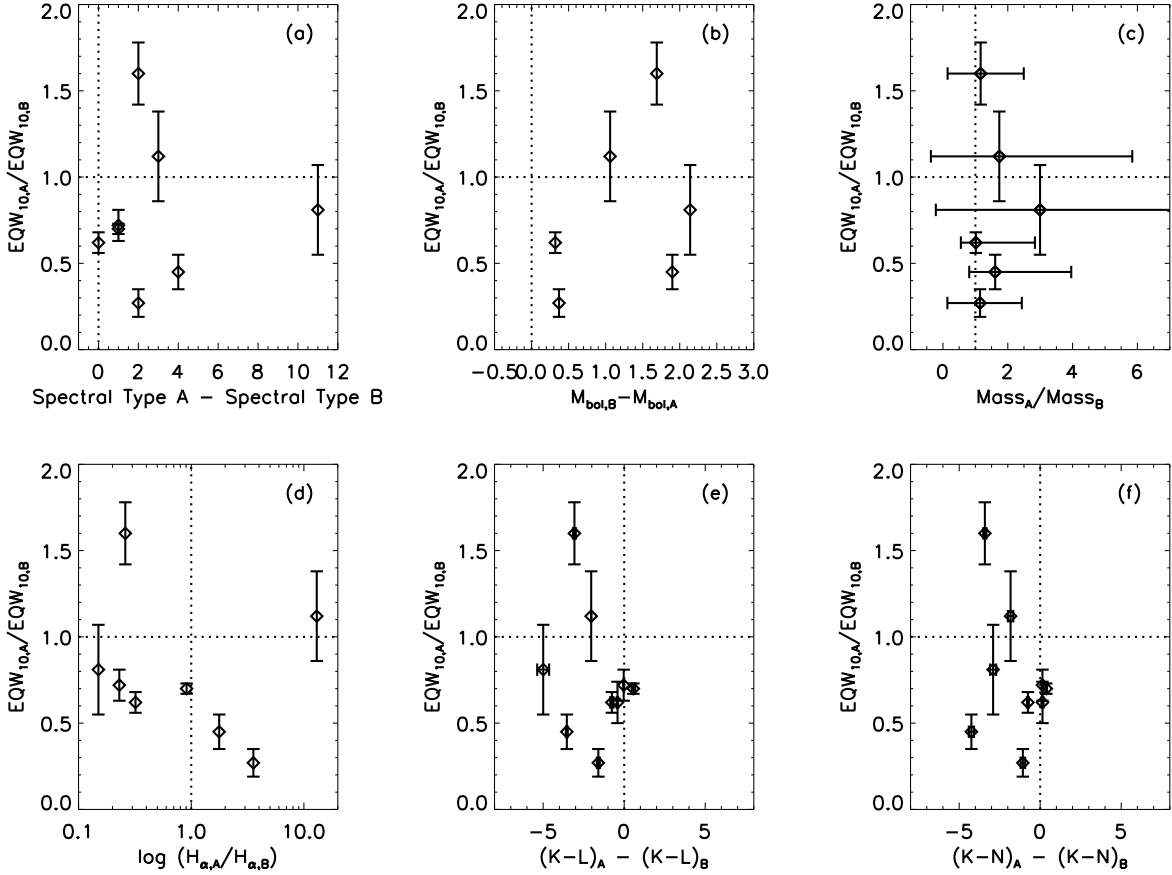


Fig. 7.— Correlations between binary star silicate feature equivalent width ratios and a set of ancillary stellar properties and disk colors. The dotted lines show equal properties between binaries. No obvious correlations are present. Frame (a) shows that in 7 out of 9 binaries, the secondary has a larger silicate feature equivalent width ($EqW_{10,A}/EqW_{10,B} < 1$). The probability that 7 or more out of 9 binaries would have larger equivalent widths in either the earlier-type components or the later-type components is 18%, which is low enough to warrant further study, but not low enough to prove a statistical difference.

REFERENCES

- Apai, D., Pascucci, I., Bouwman, J., Natta, A., Henning, T., & Dullemond, C. P. 2005, *Science*, 310, 834
- Artymowicz, P. & Lubow, S. H. 1994, *ApJ*, 421, 651
- . 1996, *ApJ*, 467, L77+
- Baraffe, I., Chabrier, G., Allard, F., & Hauschildt, P. H. 1998, *A&A*, 337, 403
- Bary, J. S., Leisenring, J. M., & Skrutskie, M. F. 2009, *ApJ*, 706, L168
- Beckwith, S. V. W. & Sargent, A. I. 1991, *ApJ*, 381, 250
- Brauer, F., Dullemond, C. P., & Henning, T. 2008, *A&A*, 480, 859
- Brusa, G., Miller, D. L., Kenworthy, M. A., Fisher, D. L., & Riccardi, A. 2004, in Presented at the Society of Photo-Optical Instrumentation Engineers (SPIE) Conference, Vol. 5490, *Advancements in Adaptive Optics*. Edited by Domenico B. Calia, Brent L. Ellerbroek, and Roberto Ragazzoni. Proceedings of the SPIE, Volume 5490, pp. 23-33 (2004)., ed. D. Bonaccini Calia, B. L. Ellerbroek, & R. Ragazzoni, 23–33
- Carrasco-González, C., Rodríguez, L. F., Anglada, G., & Curiel, S. 2009, *ApJ*, 693, L86
- Close, L. M., Biller, B., Hoffmann, W. F., Hinz, P. M., Biegging, J. H., Wildi, F., Lloyd-Hart, M., Brusa, G., Fisher, D., Miller, D., & Angel, R. 2003, *ApJ*, 598, L35
- Cohen, M., Walker, R. G., Carter, B., Hammersley, P., Kidger, M., & Noguchi, K. 1999, *AJ*, 117, 1864
- Dubrulle, B., Morfill, G., & Sterzik, M. 1995, *Icarus*, 114, 237
- Duchêne, G., Monin, J., Bouvier, J., & Ménard, F. 1999, *A&A*, 351, 954
- Dullemond, C. P. & Dominik, C. 2005, *A&A*, 434, 971
- Dutrey, A., Guilloteau, S., Duvert, G., Prato, L., Simon, M., Schuster, K., & Menard, F. 1996, *A&A*, 309, 493
- Dutrey, A., Guilloteau, S., & Simon, M. 1994, *A&A*, 286, 149
- Furlan, E., Hartmann, L., Calvet, N., D’Alessio, P., Franco-Hernández, R., Forrest, W. J., Watson, D. M., Uchida, K. I., Sargent, B., Green, J. D., Keller, L. D., & Herter, T. L. 2006, *ApJS*, 165, 568

- Furlan, E., Watson, D. M., McClure, M. K., Manoj, P., Espaillat, C., D’Alessio, P., Calvet, N., Kim, K. H., Sargent, B. A., Forrest, W. J., & Hartmann, L. 2009, *ApJ*, 703, 1964
- Ghez, A. M., Neugebauer, G., & Matthews, K. 1993, *AJ*, 106, 2005
- Glauser, A. M., Güdel, M., Watson, D. M., Henning, T., Schegerer, A. A., Wolf, S., Audard, M., & Baldovin-Saavedra, C. 2009, *A&A*, 508, 247
- Hartigan, P. & Kenyon, S. J. 2003, *ApJ*, 583, 334
- Hartigan, P., Strom, K. M., & Strom, S. E. 1994, *ApJ*, 427, 961
- Hinz, P. M., Angel, J. R. P., Woolf, N. J., Hoffmann, W. F., & McCarthy, D. W. 2000, in *Society of Photo-Optical Instrumentation Engineers (SPIE) Conference Series*, Vol. 4006, *Society of Photo-Optical Instrumentation Engineers (SPIE) Conference Series*, ed. P. Léna & A. Quirrenbach, 349–353
- Hoffmann, W. F., Hora, J. L., Fazio, G. G., Deutsch, L. K., & Dayal, A. 1998, in *Society of Photo-Optical Instrumentation Engineers (SPIE) Conference Series*, Vol. 3354, *Society of Photo-Optical Instrumentation Engineers (SPIE) Conference Series*, ed. A. M. Fowler, 647–658
- Honda, M., Kataza, H., Okamoto, Y. K., Yamashita, T., Min, M., Miyata, T., Sako, S., Fujiyoshi, T., Sakon, I., & Onaka, T. 2006, *ApJ*, 646, 1024
- Ida, S. & Lin, D. N. C. 2004a, *ApJ*, 604, 388
- . 2004b, *ApJ*, 616, 567
- Jensen, E. L. N., Dhital, S., Stassun, K. G., Patience, J., Herbst, W., Walter, F. M., Simon, M., & Basri, G. 2007, *AJ*, 134, 241
- Jensen, E. L. N., Mathieu, R. D., & Fuller, G. A. 1996, *ApJ*, 458, 312
- Juhász, A., Henning, T., Bouwman, J., Dullemond, C. P., Pascucci, I., & Apai, D. 2009, *ApJ*, 695, 1024
- Kemper, F., Vriend, W. J., & Tielens, A. G. G. M. 2004, *ApJ*, 609, 826
- Kenyon, S. J., Dobrzycka, D., & Hartmann, L. 1994, *AJ*, 108, 1872
- Kenyon, S. J. & Hartmann, L. 1995, *ApJS*, 101, 117

- Kessler-Silacci, J., Augereau, J., Dullemond, C. P., Geers, V., Lahuis, F., Evans, II, N. J., van Dishoeck, E. F., Blake, G. A., Boogert, A. C. A., Brown, J., Jørgensen, J. K., Knez, C., & Pontoppidan, K. M. 2006, *ApJ*, 639, 275
- Kessler-Silacci, J. E., Dullemond, C. P., Augereau, J., Merín, B., Geers, V. C., van Dishoeck, E. F., Evans, II, N. J., Blake, G. A., & Brown, J. 2007, *ApJ*, 659, 680
- Köhler, R., Ratzka, T., Herbst, T. M., & Kasper, M. 2008, *A&A*, 482, 929
- Kraus, A. L. & Hillenbrand, L. A. 2009, *ApJ*, 704, 531
- Kruegel, E. & Siebenmorgen, R. 1994, *A&A*, 288, 929
- Lissauer, J. J. & Stevenson, D. J. 2007, *Protostars and Planets V*, 591
- Lloyd-Hart, M. 2000, *PASP*, 112, 264
- Lommen, D. J. P., van Dishoeck, E. F., Wright, C. M., Maddison, S. T., Min, M., Wilner, D. J., Salter, D. M., van Langevelde, H. J., Bourke, T. L., van der Burg, R. F. J., & Blake, G. A. 2010, *A&A*, 515, A77+
- Luhman, K. L., Whitney, B. A., Meade, M. R., Babler, B. L., Indebetouw, R., Bracker, S., & Churchwell, E. B. 2006, *ApJ*, 647, 1180
- Mathieu, R. D., Stassun, K., Basri, G., Jensen, E. L. N., Johns-Krull, C. M., Valenti, J. A., & Hartmann, L. W. 1997, *AJ*, 113, 1841
- Mathis, J. S. 1990, *ARA&A*, 28, 37
- McClure, M. 2009, *ApJ*, 693, L81
- Meeus, G., Waters, L. B. F. M., Bouwman, J., van den Ancker, M. E., Waelkens, C., & Malfait, K. 2001, *A&A*, 365, 476
- Monin, J., Menard, F., & Duchene, G. 1998, *A&A*, 339, 113
- Natta, A., Testi, L., Calvet, N., Henning, T., Waters, R., & Wilner, D. 2007, *Protostars and Planets V*, 767
- Oliveira, I., Olofsson, J., Pontoppidan, K. M., van Dishoeck, E. F., Augereau, J., & Merin, B. 2011, *ArXiv e-prints*
- Olofsson, J., Augereau, J.-C., van Dishoeck, E. F., Merín, B., Grosso, N., Ménard, F., Blake, G. A., & Monin, J.-L. 2010, *A&A*, 520, A39+

- Ossenkopf, V. & Henning, T. 1994, *A&A*, 291, 943
- Pascucci, I., Apai, D., Hardegree-Ullman, E. E., Kim, J. S., Meyer, M. R., & Bouwman, J. 2008, *ApJ*, 673, 477
- Pascucci, I., Apai, D., Luhman, K., Henning, T., Bouwman, J., Meyer, M. R., Lahuis, F., & Natta, A. 2009, *ApJ*, 696, 143
- Piétu, V., Gueth, F., Hily-Blant, P., Schuster, K., & Pety, J. 2011, *A&A*, 528, A81+
- Przygodda, F., van Boekel, R., Àbrahàm, P., Melnikov, S. Y., Waters, L. B. F. M., & Leinert, C. 2003, *A&A*, 412, L43
- Ratzka, T., Schegerer, A. A., Leinert, C., Àbrahám, P., Henning, T., Herbst, T. M., Köhler, R., Wolf, S., & Zinnecker, H. 2009, *A&A*, 502, 623
- Riaz, B. 2009, *ApJ*, 701, 571
- Rieke, G. H. & Lebofsky, M. J. 1985, *ApJ*, 288, 618
- Roddier, C., Roddier, F., Northcott, M. J., Graves, J. E., & Jim, K. 1996, *ApJ*, 463, 326
- Sargent, B. A., Forrest, W. J., Tayrien, C., McClure, M. K., Watson, D. M., Sloan, G. C., Li, A., Manoj, P., Bohac, C. J., Furlan, E., Kim, K. H., & Green, J. D. 2009, *ApJS*, 182, 477
- Sicilia-Aguilar, A., Hartmann, L. W., Watson, D., Bohac, C., Henning, T., & Bouwman, J. 2007, *ApJ*, 659, 1637
- Simon, M., Holfeltz, S. T., & Taff, L. G. 1996, *ApJ*, 469, 890
- Skemer, A. J., Close, L. M., Hinz, P. M., Hoffmann, W. F., Greene, T. P., Males, J. R., & Beck, T. L. 2010, *ApJ*, 711, 1280
- Skemer, A. J., Close, L. M., Hinz, P. M., Hoffmann, W. F., Kenworthy, M. A., & Miller, D. L. 2008, *ApJ*, 676, 1082
- Skemer, A. J., Hinz, P. M., Hoffmann, W. F., Close, L. M., Kendrew, S., Mathar, R. J., Stuik, R., Greene, T. P., Woodward, C. E., & Kelley, M. S. 2009, *PASP*, 121, 897
- Skrutskie, M. F., Cutri, R. M., Stiening, R., Weinberg, M. D., Schneider, S., Carpenter, J. M., Beichman, C., Capps, R., Chester, T., Elias, J., Huchra, J., Liebert, J., Lonsdale, C., Monet, D. G., Price, S., Seitzer, P., Jarrett, T., Kirkpatrick, J. D., Gizis, J. E., Howard, E., Evans, T., Fowler, J., Fullmer, L., Hurt, R., Light, R., Kopan, E. L.,

- Marsh, K. A., McCallon, H. L., Tam, R., Van Dyk, S., & Wheelock, S. 2006, *AJ*, 131, 1163
- Stapelfeldt, K. R., Krist, J. E., Menard, F., Bouvier, J., Padgett, D. L., & Burrows, C. J. 1998, *ApJ*, 502, L65+
- van Boekel, R., Juhász, A., Henning, T., Köhler, R., Ratzka, T., Herbst, T., Bouwman, J., & Kley, W. 2010, *A&A*, 517, A16+
- van Boekel, R., Min, M., Waters, L. B. F. M., de Koter, A., Dominik, C., van den Ancker, M. E., & Bouwman, J. 2005, *A&A*, 437, 189
- van Boekel, R., Waters, L. B. F. M., Dominik, C., Bouwman, J., de Koter, A., Dullemond, C. P., & Paresce, F. 2003, *A&A*, 400, L21
- Watson, D. 2009, in *Astronomical Society of the Pacific Conference Series*, Vol. 414, *Cosmic Dust - Near and Far*, ed. T. Henning, E. Grün, & J. Steinacker, 77–+
- Watson, D. M., Leisenring, J. M., Furlan, E., Bohac, C. J., Sargent, B., Forrest, W. J., Calvet, N., Hartmann, L., Nordhaus, J. T., Green, J. D., Kim, K. H., Sloan, G. C., Chen, C. H., Keller, L. D., d’Alessio, P., Najita, J., Uchida, K. I., & Houck, J. R. 2009, *ApJS*, 180, 84
- Weidenschilling, S. J. 1977, *MNRAS*, 180, 57
- White, R. J. & Basri, G. 2003, *ApJ*, 582, 1109
- White, R. J. & Ghez, A. M. 2001, *ApJ*, 556, 265
- Wildi, F. P., Brusa, G., Lloyd-Hart, M., Close, L. M., & Riccardi, A. 2003, in *Society of Photo-Optical Instrumentation Engineers (SPIE) Conference Series*, Vol. 5169, *Society of Photo-Optical Instrumentation Engineers (SPIE) Conference Series*, ed. R. K. Tyson & M. Lloyd-Hart, 17–25
- Wooden, D. H., Bell, K. R., Harker, D. E., & Woodward, C. E. 2000, in *Bulletin of the American Astronomical Society*, Vol. 32, *Bulletin of the American Astronomical Society*, 1482–+
- Zsom, A., Sándor, Z., & Dullemond, C. P. 2011, *A&A*, 527, A10+